NASA TECHNICAL NOTE NASA TN D-4128

NASA TN D-4128

STUDIES OF AIRFRAME—PROPULSION-SYSTEM INTEGRATION FOR MACH 6 CRUISE VEHICLES

by Frank S. Kirkham, James M. Cubbage, Jr., Walter A. Vahl, and William J. Small

Langley Research Center
Langley Station, Hampton, Va.

NATIONAL AERONAUTICS AND SPACE ADMINISTRATION • WASHINGTON, D. C. • OCTOBER 1967

NASA TN D-4128

STUDIES OF AIRFRAME—PROPULSION-SYSTEM INTEGRATION FOR MACH 6 CRUISE VEHICLES

By Frank S. Kirkham, James M. Cubbage, Jr., Walter A. Vahl, and William J. Small

Langley Research Center
Langley Station, Hampton, Va.

NATIONAL AERONAUTICS AND SPACE ADMINISTRATION

For sale by the Clearinghouse for Federal Scientific and Technical Information
Springfield, Virginia 22151 – CFSTI price $3.00

STUDIES OF AIRFRAME—PROPULSION-SYSTEM INTEGRATION FOR MACH 6 CRUISE VEHICLES*

By Frank S. Kirkham, James M. Cubbage, Jr., Walter A. Vahl, and William J. Small
Langley Research Center

SUMMARY

An exploratory, experimental, and analytic investigation of airframe—propulsion-system integration has been conducted at a Mach number of 6. A two-pod nacelle configuration, a four-pod nacelle configuration, and a two-dimensional nacelle configuration with and without boundary-layer diverters were tested at a Reynolds number sufficient to produce a turbulent boundary layer on the wing ahead of the nacelles.

These preliminary results indicate no particular advantage of pod-type nacelles over two-dimensional designs and that the best over-all performance is obtained when the nacelle expansion area is no larger than the minimum required to enclose the turboramjet engines. A potential for significantly improving the lift-drag ratio of a configuration by utilizing the exhaust from underexpanded nozzles is also shown.

INTRODUCTION

One of the principal problems involved in the design of the hypersonic air-breathing aircraft is the efficient integration of the airframe and propulsion system. The engine airflow requirements for cruise-type aircraft designed to operate in the Mach 6 to 8 speed range are such that the inlet can be placed between the wing surface and wing-leading-edge shocks to take advantage of the high pressure airflow beneath the wing (fig. 1). At this speed, the area between the wing and shock system is large enough to permit considerable latitude in the shaping and placement of the engine nacelles (ref. 1). Some of the basic questions pertinent to this problem for Mach 6 cruise configurations are as follows:

What is the most effective exit-to-inlet area ratio for an engine housing?

Is a two-dimensional engine housing more efficient than pod-type nacelles?

Can any jet effects present be used to advantage?

The present exploratory study attempts to provide first answers to these questions, using simplified analytic and experimental models.

---

*Presented at the classified "Conference on Hypersonic Aircraft Technology," Ames Research Center, May 16-18, 1967, and published in NASA SP-148.

SYMBOLS

A_e	nacelle exit area
A_i	nacelle inlet area
$A_{i,t}$	total inlet area of a specific configuration
ΔC_D	incremental drag coefficient, Drag of wing with nacelles minus Drag of wing without nacelles
ΔC_L	incremental lift coefficient, Lift of wing with nacelles minus Lift of wing without nacelles
C_f	local skin-friction coefficient
d_i	inlet diameter (fig. 10)
h_d	height of boundary-layer diverter for two-dimensional nacelle (fig. 13)
h_i	height of inlet of two-dimensional nacelle (fig. 13)
I_{sp}	internal specific impulse, seconds
$(L/D)_{max}$	maximum lift-drag ratio
$(L/D)_o$	lift-drag ratio without jet effects
$(L/D)/(L/D)_o$	ratio of lift-drag ratio with jet effects to lift-drag ratio without jet effects
l_{strut}	length of pod support strut (fig. 10)
M_∞	free-stream Mach number
p_e	nozzle exit static pressure
p_l	static pressure under wing
R_l	local Reynolds number
S_w	wing planform area
α	angle of attack, degrees
ϵ	wing reflex angle, degrees (fig. 18)
θ	diverter wedge angle, degrees (fig. 13)

RESULTS AND DISCUSSION

Engine Nacelle Sizing Requirements

As a starting point, consider the size engine and inlet required for cruising flight at Mach 6. A representative thrust-drag schedule for the acceleration trajectory of a Mach 6 cruise vehicle is presented in figure 2. In-line subsonic combustion turboramjets are used with the transition from turbojet to ramjet operation occurring at approximately Mach 3. In determining the size of the propulsion system required, the turbojet thrust must be adequate to provide the minimum acceleration desired in the pinch regions occurring either during the subsonic climb which may be imposed due to sonic-boom consideration or during the transonic acceleration. The ramjet thrust and the inlet area required are usually tailored to the cruise conditions, provided that satisfactory performance can be obtained over the complete acceleration trajectory. Once the thrust requirements and hence the engine size have been determined, the minimum propulsion pod dimensions are established - that is, the pod inlet area and engine exhaust nozzle exit area.

A parametric variation of the ratio of nozzle-exit static pressure p_e to underwing static pressure p_1 is given as a function of nacelle expansion ratio A_e/A_i in figure 3. These curves are generally applicable for subsonic combustion ramjets and are constant over a range of altitude provided that the maximum duct internal pressure limit is not exceeded. Also shown are the results from an in-house mission-analysis computer program which sizes the engine for a particular set of vehicle aerodynamics. The aerodynamics used herein were obtained from the study results of the distinct delta wing and blended wing-body cruise configurations described in reference 2. The sizes of both in-line and wrap-around turboramjet engines required are indicated by bars in the figure for an altitude of approximately 100 000 ft. The lengths of these bars indicate the variation obtained as the aircraft configuration was changed from the distinct wing-body concept with a wing loading of 76 lb/ft^2 ($\alpha \approx 7^\circ$) to a blended wing-body concept with a wing loading of 42 lb/ft^2 ($\alpha \approx 5^\circ$). The minimum nacelle expansion ratio required for the in-line engine is about 1.3. The wrap-around engine is somewhat larger and requires a nacelle expansion ratio of about 1.7. The nozzle exhausts are underexpanded $\left(p_e/p_1 > 1\right)$ for both engine types and nacelle expansion ratios on the order of 2.5 would be required to achieve full expansion.

As shown in figure 4, about a 5-percent increase in internal specific impulse can be obtained by fully expanding the nozzle exhausts. If the nozzle flow can be expanded into the wing surface, this increased engine performance might be obtained with no penalty in aerodynamic drag. If, however, the frontal area of the nacelle must be enlarged to achieve full expansion, the increase in engine performance with increasing nacelle exit-to-inlet area ratio must be traded off against the attendant drag penalty of an enlarged nacelle.

Aerodynamic Characteristics

A wind-tunnel program to examine the aerodynamic characteristics of various nacelle configurations was initiated. The types of nacelles considered are shown in figure 5. Tests were conducted in the Langley 20-inch Mach 6 tunnel with a sharp leading-edge 70° sweep delta wing. (A description of the wind tunnel is given in ref. 3.) Flow-through nacelles with constant internal duct areas were used to simulate a two-pod nacelle configuration, a four-pod nacelle configuration, and a two-dimensional nacelle configuration. The total inlet area was 1.8 percent of the wing planform area for all configurations. Neither the inlet compression surfaces nor the correct nozzle exhaust flow were simulated in this investigation. The pod external contour was parabolic with a 14° initial angle at the lip. The distance between adjacent pod center lines was 2 inlet diameters and the pods were 5 diameters long for all pod configurations tested. The pods were placed longitudinally so that the outboard pods would be behind the wing shocks throughout the angle-of-attack range ($0° \leq \alpha \leq 8°$).

It was determined experimentally (ref. 4) that the boundary layer on the wing is fully turbulent in the hatched region shown in the sketches. The nacelles were tested in this region of fully turbulent wing boundary layer. The boundary layer on the two-dimensional and four-pod engine nacelles is believed to be transitional while a region of fully turbulent flow probably existed on the rearmost portion of the two-pod engine nacelles.

The importance of testing with turbulent boundary layers is illustrated in figure 6. The relative drag penalties of two-dimensional nacelles and pod nacelles are shown for both laminar and turbulent wing boundary layers. Tests conducted in the Langley 11-inch hypersonic tunnel at Mach 6.8 where the wing boundary layer was laminar indicate that the pod-nacelle installation has 50 percent more drag than the two-dimensional nacelle. Earlier results of this kind were interpreted as virtually ruling out the use of pods on hypersonic vehicles (ref. 1). However, tests at Mach 6 with turbulent wing boundary layers show the pods to have only a 20-percent drag penalty relative to the two-dimensional installation and this can probably be further reduced with refinements in design. Thus, by testing with the correct type of boundary layer, the pod nacelle is restored to a more competitive position relative to the two-dimensional design. The Reynolds number for the Mach 6 tests is still only 5 percent of the full-scale flight Reynolds number and, thus, additional scale effects may be expected.

The results obtained in the wind-tunnel program are presented in figures 7 to 16. For two-pod nacelles, the effect of increasing the nacelle expansion ratio is shown in figure 7. The oil-flow photograph shows that a strong interaction occurs between the nacelle shocks and the wing surface which produces significant interference forces on the wing and nacelles.

The increments in lift and drag obtained when the nacelles are added to the basic wing are shown as a function of α in figure 7. These data were obtained with a six-component strain-gage balance. All data are corrected for nacelle internal drag and for nacelle base drag. The internal drag correction was obtained by calculating the internal skin friction with the assumption of

a laminar boundary layer. The base pressure was corrected to free-stream static pressure by assuming that the base pressure coefficient in the wind-tunnel tests was equal to $-1/M_\infty^2$.

The theoretical predictions, shown as dashed curves, consisted of an estimate of the external pressure and friction drag on the nacelles and their support struts plus an estimate of the forces on the wing in the interference region. The pressure forces on the pod nacelles were calculated by the method of characteristics for axisymmetric rotational flow. Shock-expansion theory was used on the support struts. The drag of all leading edges was obtained from Newtonian theory with a maximum pressure coefficient of 1.2. The interference pressures on the wing were obtained from the pressure distribution in the axisymmetric flow field in the plane of the wing. Skin friction on the nacelles was assumed laminar for calculation purposes and to follow the equation $C_f\sqrt{R_l} = 0.625$. The theory predicts the trends but not the magnitude of the experimental data.

The increments in lift and drag were used with the drag polar obtained from wind-tunnel tests of the delta-wing hypersonic cruise vehicle configuration described in reference 5 to obtain the effects of engine nacelle modifications on the maximum untrimmed lift-drag ratio for a practical cruise vehicle design. The results are shown in figure 8. Addition of two pods with an expansion ratio of 1.5 decreased the maximum L/D from about 4 to 3.8 while increasing the nacelle expansion ratio to 2 decreased maximum L/D to about 3.6.

The effect of changing the length of the pod support strut is shown in figure 9. At low angles of attack, the incremental lift ΔC_L is increased as pods are pulled closer to the wing surface but the incremental drag is unchanged. The drag is affected at the higher angles because the contribution of normal force to drag becomes significant. When these increments are applied to the delta-wing cruise configuration (fig. 10) only a slight benefit in $(L/D)_{max}$ is obtained by decreasing the strut length because $(L/D)_{max}$ occurs at about $\alpha = 8^\circ$. A higher performance configuration with $(L/D)_{max}$ occurring at lower angles of attack ($\alpha \leq 4^\circ$) would benefit more from short pod support struts because additional lift could be obtained with no increase in drag. Thus, pod nacelles should be placed as close to the wing surface as is practical and perhaps merged into the wing surface.

A four-pod nacelle configuration is compared with the two-pod nacelle configuration in figure 11. The theory, contrary to the data, predicts a larger ΔC_L for the four-pod configuration than for the two-pod configuration. This discrepancy is possibly a result of the nacelles being placed farther forward from the wing trailing edge (relative to the length of the nacelle) for the four-pod configuration than the nacelles of the two-pod configuration. Both force and pressure tests to determine the effects of varying longitudinal placement of pod-type nacelles are needed to see whether significant changes in the aerodynamic forces occur. The theory does, however, predict an increase in drag as the number of pods is increased as would be expected since the wetted

area and leading-edge area increase as the number of pods increases. The effects of these increments on $(L/D)_{max}$ are shown in figure 12.

The results of the investigation of a two-dimensional nacelle with an exit-to-inlet area ratio of 1.5 are shown in figures 13 to 15. The nacelle was tested with and without boundary-layer diverters. Without diverters, the nacelle was mounted flush with the wing surface and the wing boundary layer was allowed to flow through the nacelle. The lower surface of the nacelle was a circular-arc profile with an initial angle of 8.4°. The side plates were swept 75° with sharp leading edges and a 5° wedge angle.

Boundary-layer diverters may be used to avoid degrading engine performance due to ingesting the wing boundary layer. To simulate boundary-layer diverters, the two-dimensional nacelle was supported on two struts (fig. 13). The upper surface of the nacelle had a 5° wedge angle which diverted the wing boundary layer toward the wing surface. The center portion of the boundary layer flowed through a constant area duct between the wing and nacelle, whereas the outer portion was diverted toward the sides of the nacelles by the wedges on the diverters. The diverter height was sized such that the entire wing boundary layer in the wind-tunnel model would be diverted away from the inlet. On a flight vehicle the wing boundary layer would be relatively 60 percent as thick as in the wind tunnel and the diverter height could be correspondingly reduced. The curved shocks produced by the diverters (shown in the photograph) indicate that there is a complicated interaction between the wing, the diverter, and the nacelle which may be in part caused by choking in the diverter duct and boundary-layer separation.

The lift and drag increments for this configuration are shown in figure 14. The theoretical prediction of the forces on the lower surface of the nacelle was obtained by using two-dimensional shock-expansion theory with a correction for edge effects by the method of reference 6. The theoretical predictions of the effects of adding boundary-layer diverters were done by first finding the equivalent Mach number in the turbulent wing boundary layer at the forward face of the two-dimensional inlet (ref. 7). The flow was assumed inviscid aft of this point and the pressures were calculated by shock-expansion theory using the equivalent boundary-layer Mach number as a starting point. The skin friction in the diverter ducts was assumed turbulent and calculated by the T' method described in reference 8. The seemingly accurate predictions of lift and drag given in figure 14 are fortuitous since the axial force was underpredicted and the normal force overpredicted which tended to compensate each other when lift and drag were calculated.

The effect of these increments on $(L/D)_{max}$ is shown in figure 15. The two-dimensional nacelle without boundary-layer diverters caused only a small loss in $(L/D)_{max}$ in spite of the fact that the lower surface of the nacelle was contoured to give an exit-to-inlet area ratio of 1.5. When diverters are added, however, a significant penalty in $(L/D)_{max}$ is incurred. This penalty is unchanged by reducing the diverter height by about 30 percent. Increasing the diverter wedge angle from 5° to 10° reduced $(L/D)_{max}$ as expected.

A comparison of the various nacelle concepts is shown in figure 16. The best aerodynamic performance was obtained with the two-dimensional nacelle without boundary-layer diverters. The addition of boundary-layer diverters, however, decreased the performance of the two-dimensional nacelle to below that of the two-pod nacelle configuration. More carefully designed diverters would undoubtedly increase this performance level but the drag penalty for pod nacelle installations can also probably be reduced by proper integration of the pods and aircraft. Some of the pertinent variables for integrating pod nacelles with the aircraft at lower speeds ($M \approx 3$) are described in references 9 to 12. Since additional work to optimize both nacelle types is needed, no clear-cut choice between two-dimensional nacelles and pod nacelles can be made at this time.

The trade-off between the increase in engine performance against the decrease in aerodynamic performance as the nacelle expansion ratio is increased can now be examined. The pertinent parameter $(L/D)_{max}(I_{sp})$ is shown on the right of figure 16. Assuming expansion of the nozzle flow into the wing surface and no increase in external drag, the two-dimensional nacelle without boundary-layer diverters can obtain a $2\frac{1}{2}$ percent gain in performance as A_e/A_i is increased from 1.5 to 2. This increase is due solely to increasing I_{sp} and the degradation in engine performance due to boundary-layer ingestion has not been included for this configuration. This performance level would be reduced if boundary-layer ingestion effects were included. For the two-pod configuration, the increase in drag with increasing expansion ratio more than counterbalances the improvement in engine performance, and the best over-all performance is obtained with the low area ratio nacelle. Considering the small performance gains obtainable by additional nozzle expansion, it appears that the nozzle exits should not be enlarged beyond the minimum size required by the engine. If the nozzle exit areas are thus restricted, the nozzle exhaust flow will be underexpanded as was discussed in conjunction with figure 3. The flow from underexpanded nozzles may impinge on adjacent aircraft surfaces and produce jet interference forces on the aircraft. A preliminary estimate of the jet interference effects on the blended wing-body configuration has been made and is considered next.

Jet Interference Effects

The configuration shown in figure 17 is the blended wing-body concept. Further description of this configuration is given in reference 5. The nacelle housing the engines is 30 ft wide and the nozzle exits are 40 ft upstream of the wing trailing edge. If the nozzle exit pressure p_e is greater than the underwing static pressure p_1 the nozzle flow continues to expand along the surface of the wing creating an interference pressure field and a resulting force on the wing. In the flow model used to obtain a preliminary estimate of these forces, the flow was assumed to be two dimensional, the wing to be flat, and the pressure p_e to be constant along the wing surface to the point where the trailing expansion wave strikes the wing.

An example jet effect calculation utilizing these assumptions is illustrated in figure 18 where the ratio L/D with jet effects to L/D without jet effects is plotted as a function of the wing reflex angle ϵ. Significant improvements in L/D can be achieved throughout the range of static-pressure ratios considered without reflexing the wing. Wing reflex has a small beneficial effect at the higher pressures but is detrimental at lower pressures. A discussion of the utilization of underexpanded exhausts from asymmetric nozzles is given in reference 13.

The effect of jet interference on L/D that might be obtained with realistic engines was determined through a range of cruise Mach numbers from 5 to 8, as shown in figures 19 and 20. In figure 19, the static-pressure ratios for both in-line and wrap-around turboramjet engines, as obtained by the methods discussed in conjunction with figure 3, are shown as a function of cruise Mach number. Both engine types have underexpanded nozzle exhausts throughout this Mach number range. The L/D improvements obtained by utilizing these exhaust overpressures range from 5 to 15 percent for the in-line engines and from 3 to 10 percent for the wrap-around engines (fig. 20). Some of the implications of these interference forces on aircraft stability are discussed in reference 5.

Although these L/D improvements were obtained from an idealized analytical flow model, it is apparent that significant improvement in L/D can probably be realized by proper utilization of the exhausts of underexpanded nozzles. Because of the extreme complexity of the exhaust flow field, a more realistic assessment of these effects must be obtained through experimental tests.

CONCLUDING REMARKS

These exploratory studies of airframe—propulsion-system integration at Mach 6 have revealed that underexpanded nozzles, whose exit areas are no larger than the maximum area required by the engine, appear to produce better over-all performance than fully expanded nozzles. Preliminary calculations indicate that underexpanded nozzles exhausting well ahead of the wing trailing edge have a significant potential for increasing the lift-drag ratio. These jet exhaust effects, however, require detailed experimental verification.

In regard to nacelle type, these preliminary results indicated no particular advantage of two-dimensional designs over individual pods.

The important interference effects of the nacelles on both lift and drag at hypersonic speeds were in general not predicted accurately by the simple analytic techniques currently in use.

Langley Research Center,
National Aeronautics and Space Administration,
Langley Station, Hampton, Va., May 16, 1967,
126-13-03-31-23.

REFERENCES

1. Fetterman, David E.; McLellan, Charles H.; Jackson, L. Robert; Henry, Beverly Z., Jr.; and Henry, John R.: A Review of Hypersonic Cruise Vehicles. NASA TM X-1276, 1966.

2. Drake, Hubert M.; Gregory, Thomas J.; and Petersen, Richard H.: Hypersonic Technology Problems Identified in Mission Studies. Conference on Hypersonic Aircraft Technology, NASA SP-148, 1967, pp. 1-19.

3. Sterrett, James R.; and Emery, James C.: Extension of Boundary-Layer-Separation Criteria to a Mach Number of 6.5 by Utilizing Flat Plates With Forward-Facing Steps. NASA TN D-618, 1960.

4. Sterrett, James R.; Morrisette, E. Leon; Whitehead, Allen H., Jr.; and Hicks, Raymond M.: Transition Fixing for Hypersonic Flow. Conference on Hypersonic Aircraft Technology, NASA SP-148, 1967, pp. 203-222. (Also available as NASA TN D-4129.)

5. Penland, Jim A.; Edwards, Clyde L. W.; Witcofski, Robert D.; and Marcum, Don C., Jr.: Comparative Aerodynamic Study of Two Hypersonic Cruise Aircraft Configurations Derived From Trade-Off Studies. Conference on Hypersonic Aircraft Technology, NASA SP-148, 1967, pp. 45-62. (Also available as NASA TM X-1436.)

6. Liepmann, H. W.; and Roshko, A.: Elements of Gasdynamics. John Wiley & Sons, Inc., c.1957.

7. Pinckney, S. Z.: Semiempirical Method for Predicting Effects of Incident-Reflecting Shocks on the Turbulent Boundary Layer. NASA TN D-3029, 1965.

8. Peterson, John B., Jr.: A Comparison of Experimental and Theoretical Results for the Compressible Turbulent-Boundary-Layer Skin Friction With Zero Pressure Gradient. NASA TN D-1795, 1963.

9. Nichols, Mark R.: Aerodynamics of Airframe-Engine Integration of Supersonic Aircraft. NASA TN D-3390, 1966.

10. Swan, Walter C.: A Discussion of Selected Aerodynamic Problems on Integration of Propulsion Systems With Airframe on Transport Aircraft. Aerodynamics of Power Plant Installation, Part 1, AGARDograph 103, Oct. 1965, pp. 23-68.

11. Robins, A. Warner; Morris, Odell A.; and Harris, Roy V., Jr.: Recent Research Results in the Aerodynamics of Supersonic Vehicles. J. Aircraft, vol. 3, no. 6, Nov.-Dec. 1966, pp. 573-577.

12. Landrum, Emma Jean: Effect of Nacelle Orientation on the Aerodynamic Characteristics of an Arrow Wing-Body Configuration at Mach Number 2.03. NASA TN D-3284, 1966.

13. Lewis, W. G. E.; Herd, R. J.; and Herbert, M. V.: Lift Characteristics of Asymmetric Exhaust Nozzles at High Flight Speeds. J. Roy. Aeron. Soc. (Tech. Notes), vol. 70, no. 671, Nov. 1966, pp. 1036-1040.

MACH 6 CRUISE CONFIGURATION

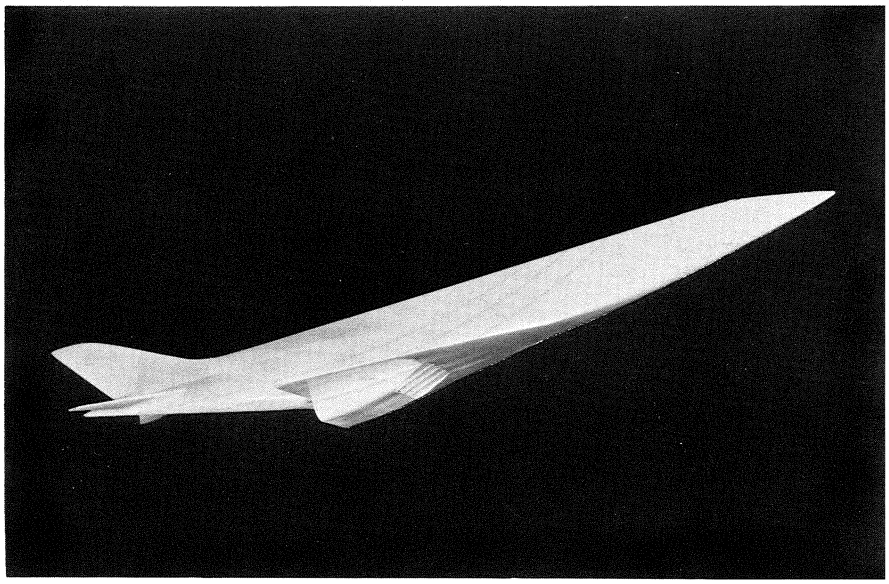

Figure 1 L-2871-19

TYPICAL THRUST – DRAG SCHEDULE
IN-LINE TURBORAMJET

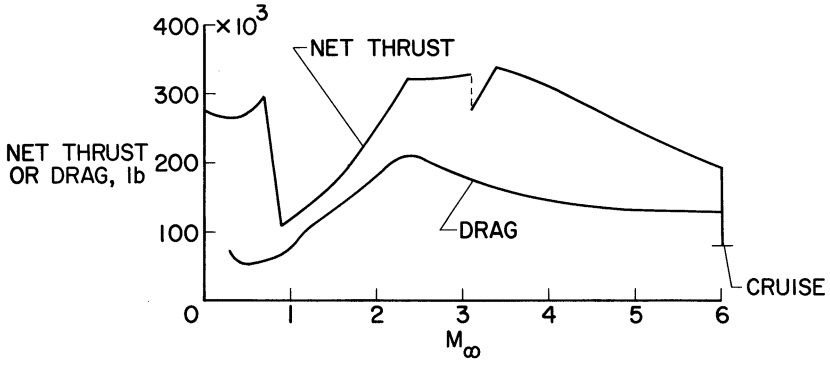

Figure 2

NOZZLE-EXIT STATIC-PRESSURE RATIOS AT $M_\infty=6$

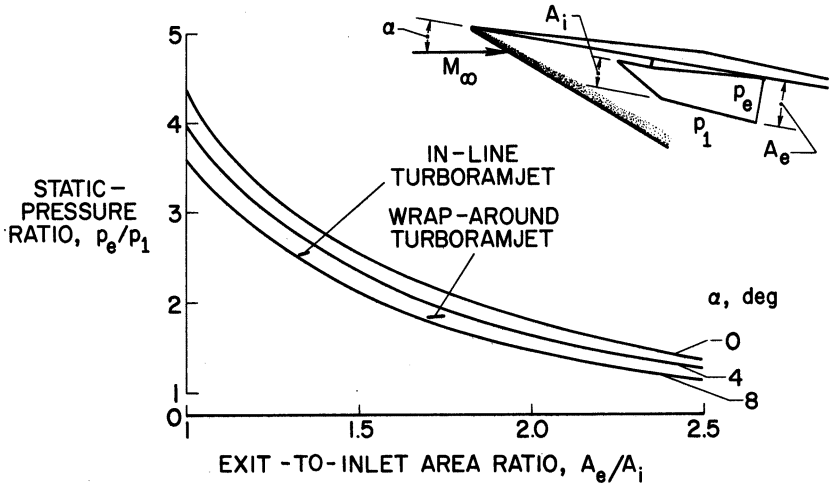

Figure 3

RAMJET SPECIFIC IMPULSE
$M_\infty=6$

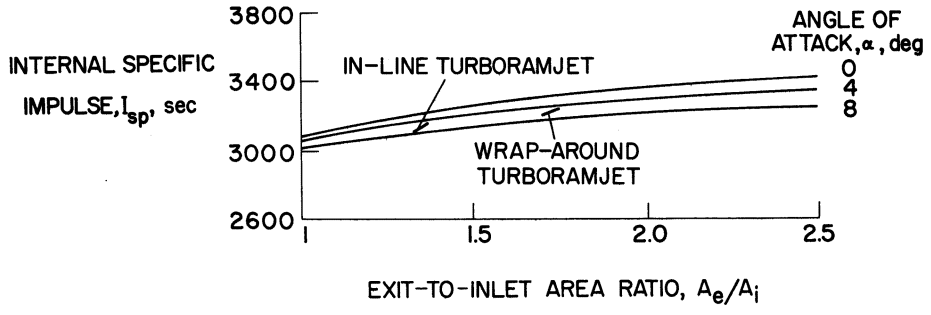

Figure 4

NACELLE CONFIGURATIONS INVESTIGATED

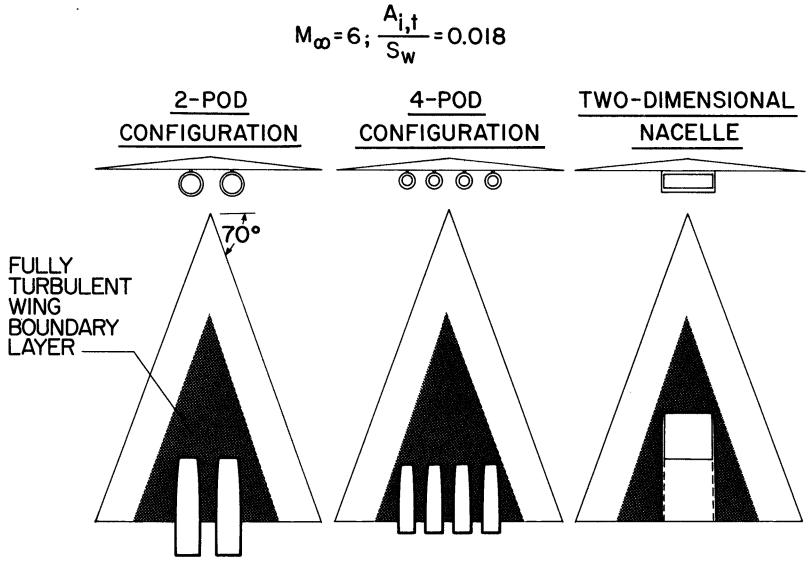

Figure 5

COMPARISON OF NACELLE DRAG IN LAMINAR AND TURBULENT FLOW

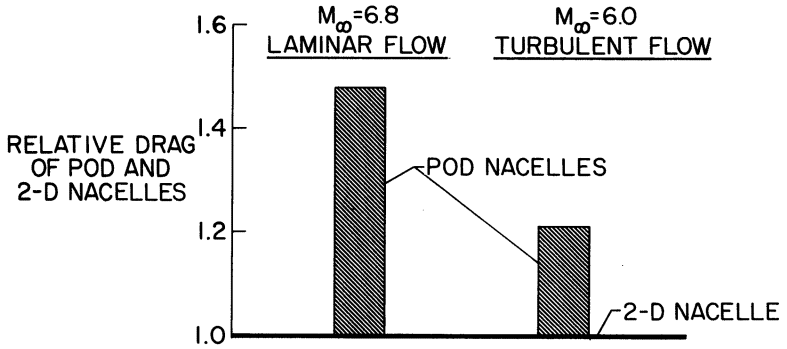

Figure 6

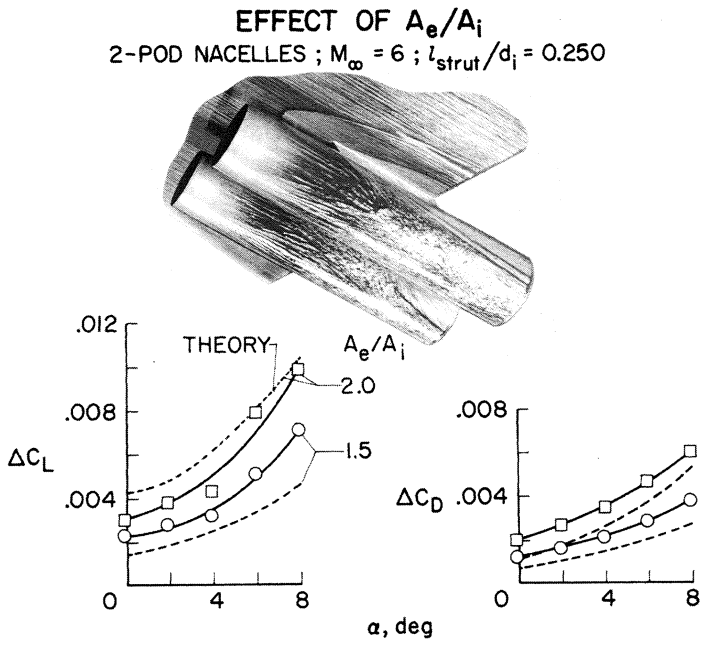

Figure 7

L-2871-4

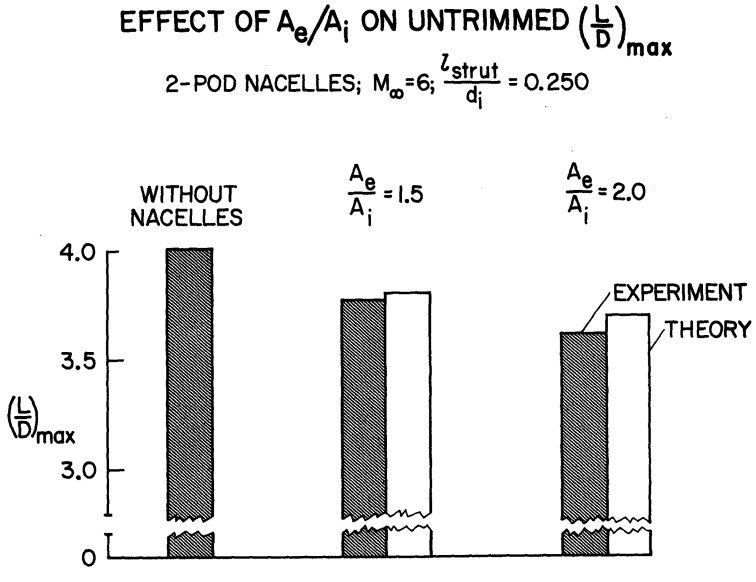

Figure 8

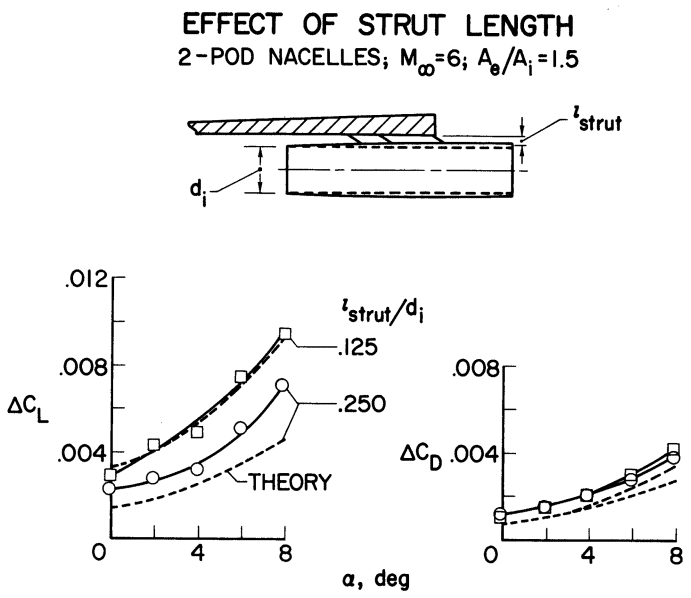

Figure 9

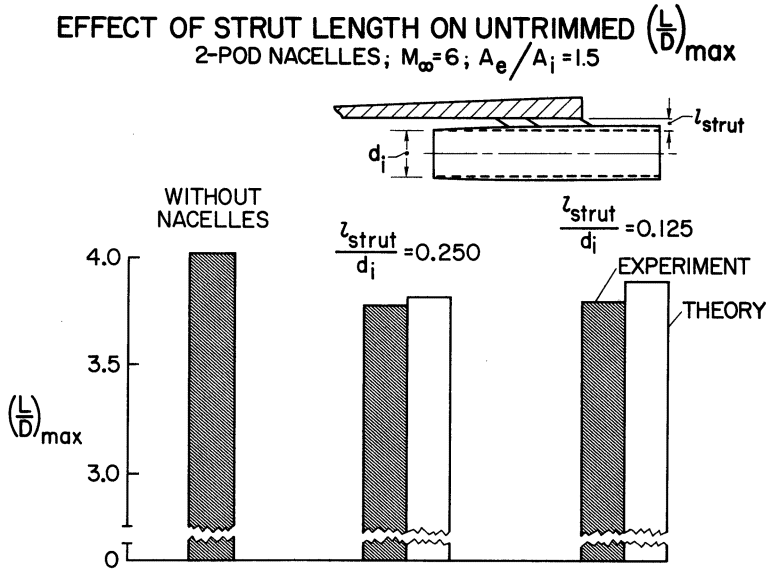

Figure 10

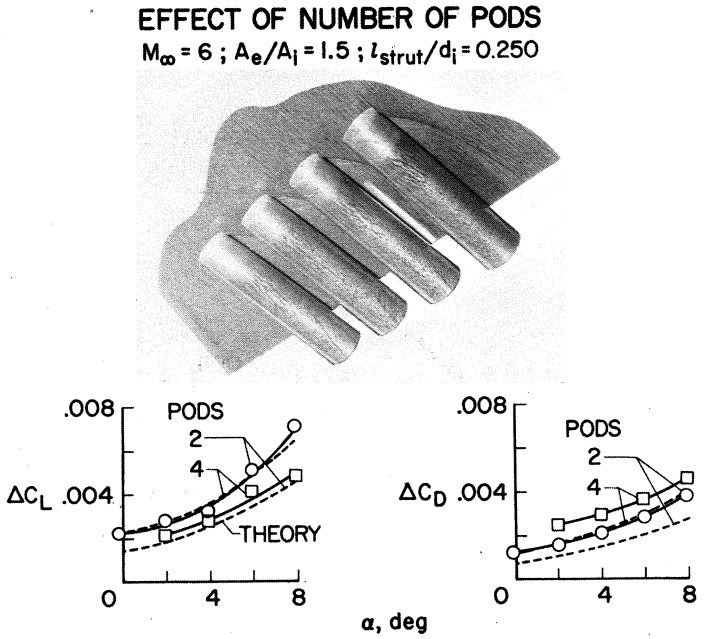

Figure 11

L-2871-8

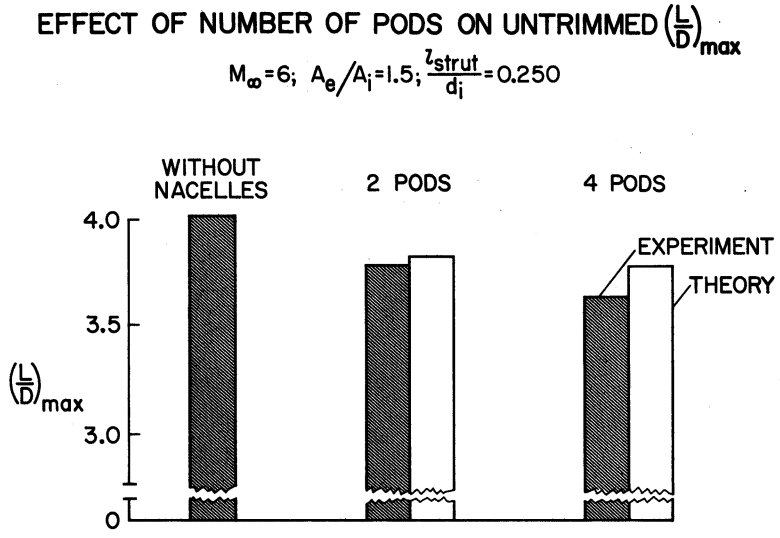

Figure 12

TWO-DIMENSIONAL NACELLE WITH
FLOW-THROUGH DIVERTER
$A_e/A_i = 1.5$

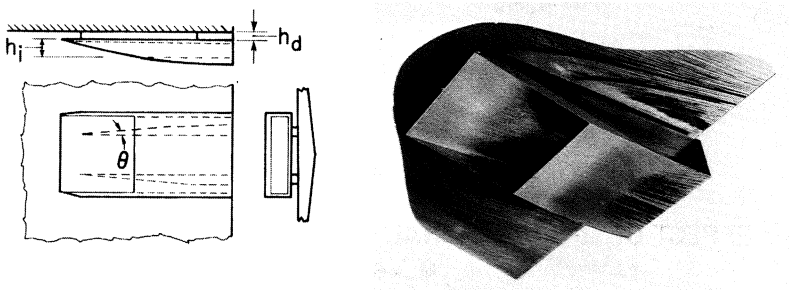

Figure 13 L-2871-10

EFFECT OF 2-DIMENSIONAL NACELLE ON LIFT AND DRAG

$M_\infty = 6$ $A_e/A_i = 1.5$

DATA	THEORY	TYPE DIVERTER
○	———	WITHOUT DIVERTER
□	—·—	$\theta = 5°$ $h_d/h_i = 0.29$
◇	— - —	$\theta = 5°$ $h_d/h_i = 0.17$
△	-------	$\theta = 10°$ $h_d/h_i = 0.29$

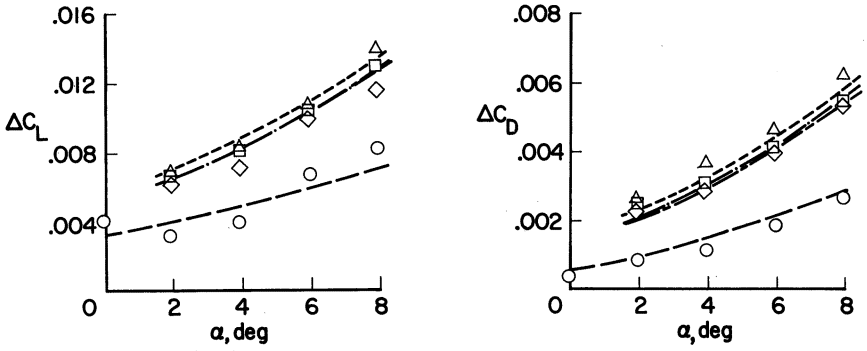

Figure 14

EFFECT OF 2-DIMENSIONAL NACELLES ON UNTRIMMED $\left(\frac{L}{D}\right)_{max}$

$M_\infty = 6$; $A_e/A_i = 1.5$

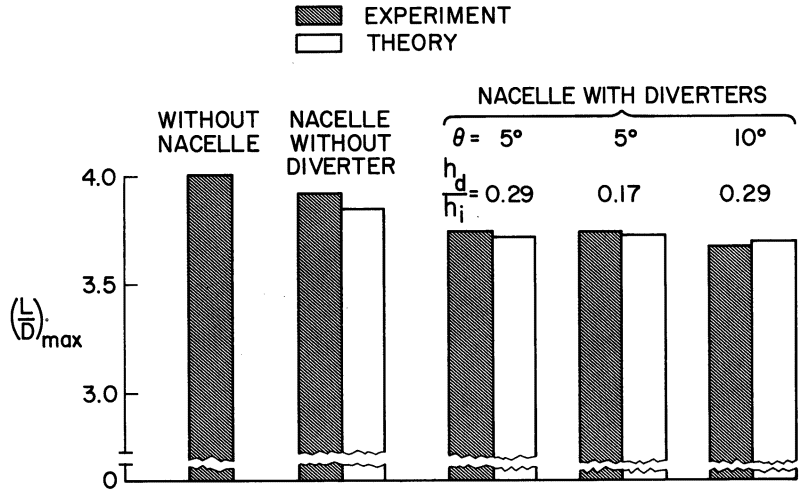

Figure 15

SUMMARY OF 2-DIMENSIONAL AND POD NACELLE PERFORMANCE

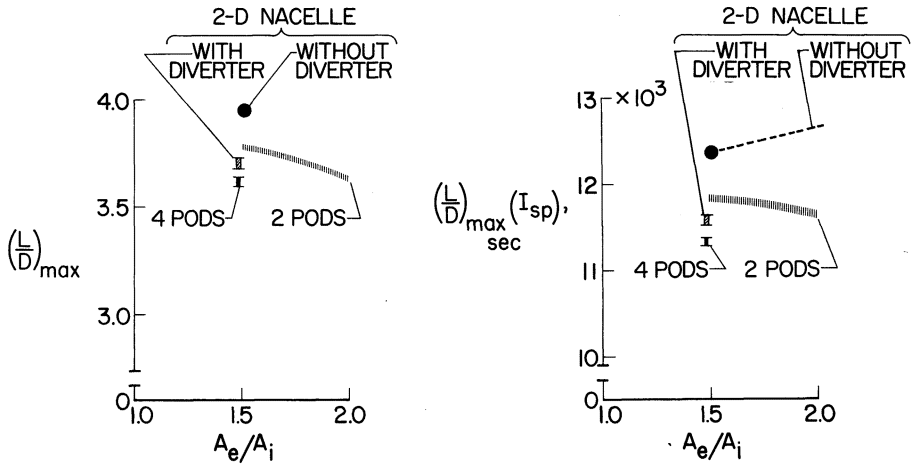

Figure 16

JET-INTERFERENCE FLOW MODEL

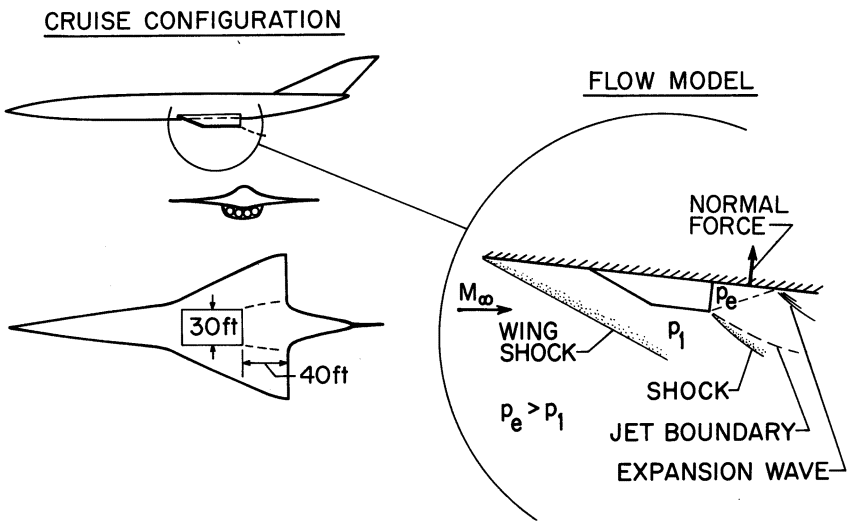

Figure 17

EFFECT OF JET INTERFERENCE ON $\frac{L}{D}$

$M_\infty = 6$; ALTITUDE = 100000 ft ; $\left(\frac{L}{D}\right)_o = 5$

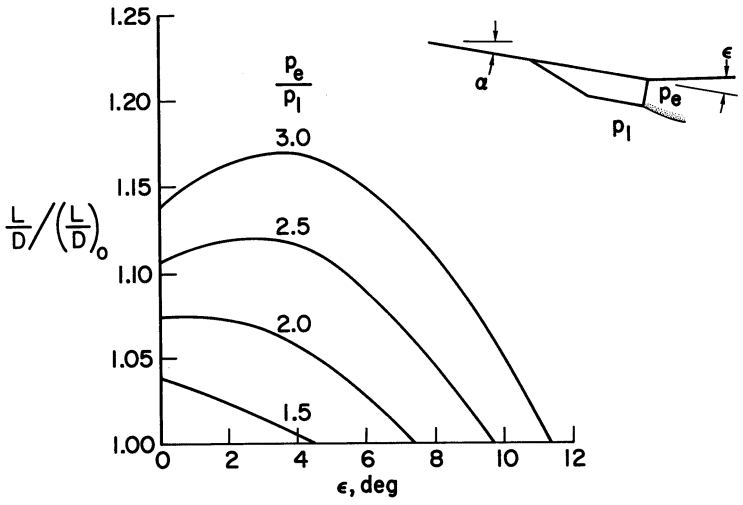

Figure 18

NOZZLE-EXIT STATIC-PRESSURE RATIOS AT CRUISE

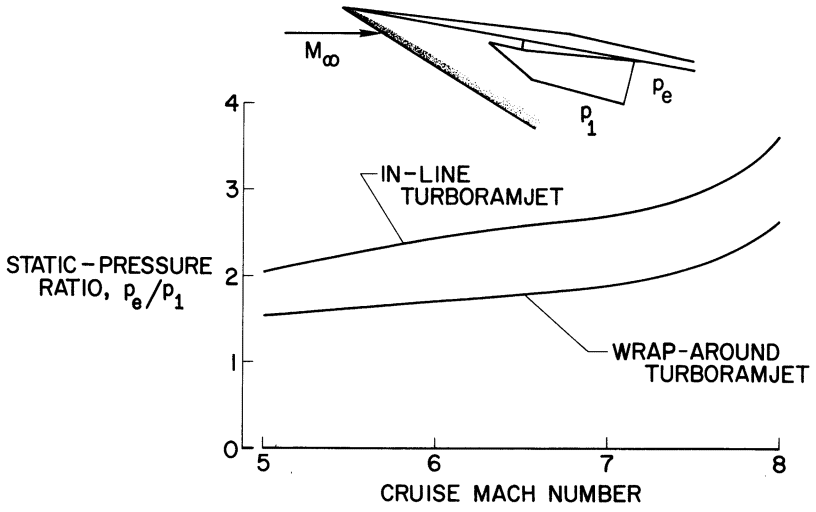

Figure 19

$\frac{L}{D}$ IMPROVEMENT DUE TO ENGINE-EXHAUST-WING INTERFERENCE

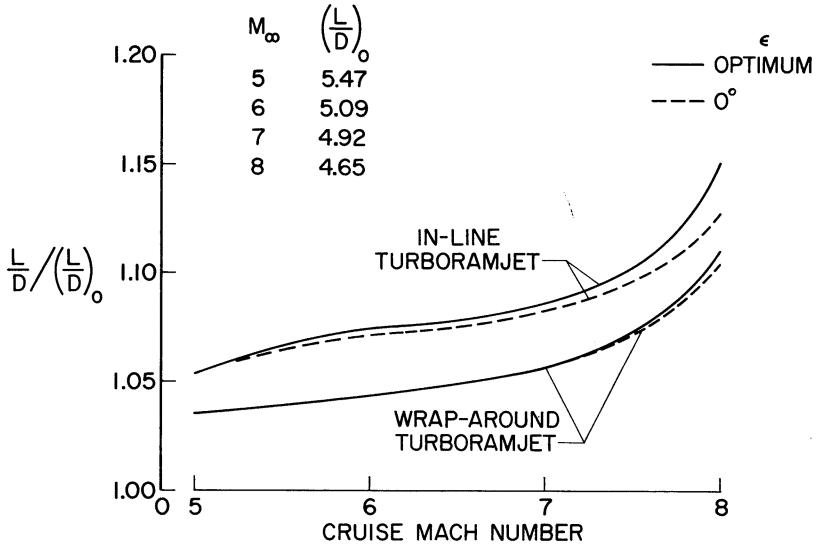

Figure 20